CLM-R 65

CLM-R 65

United Kingdom Atomic Energy Authority

RESEARCH GROUP

Report

ANNULAR PLASMAS PRODUCED BY ROTATING MAGNETIC FIELDS

P. A. DAVENPORT
G. FRANCIS
W. MILLAR
A. F. TAYLOR

Culham Laboratory
Abingdon Berkshire

1966

Available from H. M. Stationery Office

FOUR SHILLINGS NET

U.D.C.
621.039.629

UNCLASSIFIED
(Approved for sale)

CLM - R 65

ANNULAR PLASMAS PRODUCED BY ROTATING MAGNETIC FIELDS

by

P.A. DAVENPORT
G. FRANCIS
W. MILLAR
A.F. TAYLOR

A B S T R A C T

A rotating magnetic field was applied to a cylindrical plasma in a discharge tube whose walls were electrically conducting in the azimuthal direction, which imposed the constraint that the net axial magnetic flux in the tube remained constant. A theoretical analysis of the system predicts that the plasma should be confined in an annular configuration, and this was confirmed experimentally by observations using magnetic probes, an image-converter camera and a laser interferometer. A detailed description of the circuits used to pre-ionize the plasma and to produce the rotating field is appended.

U.K.A.E.A. Research Group,
Culham Laboratory,
Nr. Abingdon,
Berks.

August, 1966 (C.18 ED,MEA)

CLM-R 82

UNCLASSIFIED
(Approved for sale)

CONTENTS

NOTATION

Electromagnetic units are used and symbols common to this report and CLM-R 12 have the same meaning.

r, θ, z	cylindrical co-ordinates
B	magnetic field
B_a	applied axial magnetic field
B_1	axial magnetic field of wall currents
B_o	rotating magnetic field amplitude
B^*	$B_1 + B_a$
j	current density
K	radial distribution parameter
n	electron density
n_o	maximum value of n
N_o	electron line density
N	electron line density outside a cylinder of radius r
η	resistivity
r_e	classical electron radius
r_o	radius of maximum density
Δr	half-width of annulus
R	wall radius
T_e, T_i	electron, ion temperature
T	$T_e + T_i$
τ_e, τ_i	electron, ion collision interval
ω	angular frequency of rotating field
ω_e, ω_i	electron, ion cyclotron frequencies in B_o
ω_{ea}	electron cyclotron frequency in B_a

INTRODUCTION

It has been shown[1,2,3] that the application of a rotating magnetic field to a cylindrical plasma can produce large azimuthal electron currents, provided that the angular frequency of the rotating field lies between the ion and electron cyclotron frequencies, and the electron collision frequency is less than the electron cyclotron frequency. If a steady axial magnetic field is also applied, the radial Lorentz force can confine the plasma away from the tube walls.

A simple analysis of the system can be made on the assumption that all the electrons are tied to the lines of force of the rotating field and circulate synchronously with its angular velocity ω, whereas the ions have no net azimuthal motion. The electrons thus form a cylindrical current sheet, and if the electron line density is N_o per cm length the magnetic field of the sheet changes by $2N_o e\omega$ as we pass from the axis to the wall. We now consider the superposition of this magnetic field and an applied axial magnetic field B_a. Three distinct situations can arise (Fig.1):-

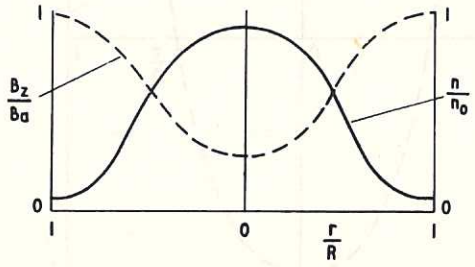

Fig. 1(a) $2N_o e\omega < B_a$ (CLM-R65)

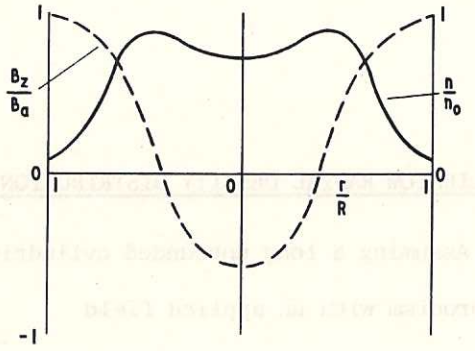

Fig. 1(b) $2B_a > 2N_o e\omega > B_a$ (CLM-R65)

(i) If $2N_o e\omega < B_a$ the magnetic field decreases continuously from the wall towards the axis. To preserve pressure balance the electron density is a maximum on the axis and decreases steadily outwards.

(ii) If $2N_o e\omega > B_a$ but $< 2B_a$ the magnetic field at the axis is reversed. The electron density is a maximum at some intermediate radius r_o where the magnetic field passes through zero.

(iii) If $2N_o e\omega > 2B_a$ the inner reversed field exceeds the outer field and the current sheet is pushed out to the walls; no containment is possible.

This general behaviour was observed by Blevin and Thonemann[1].

Our experiments were designed to remove the restriction (iii) on the maximum value of N_o for which the plasma can be confined. This can be achieved by making the outer surface of the tube wall electrically conducting in the azimuthal direction, which conserves

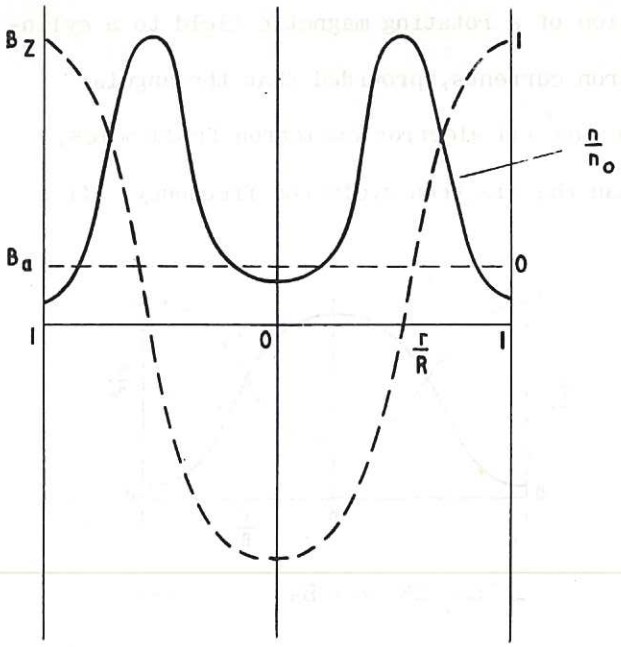

Fig. 2 $N_o e\omega \gg B_a$: flux conserved (CLM-R65)

the net axial flux enclosed by the wall while still allowing the rotating field to penetrate the plasma. Theory now predicts that for all values of $N_o e\omega > B_a$ the plasma will assume an annular configuration similar to that in situation (ii) above, the radius of maximum density tending to $1/\sqrt{2}$ of the wall radius as $N_o e\omega/B_a \to \infty$ (Fig. 2).

Our observations are in substantial agreement with the theoretical predictions of annular plasma containment, developed below, and show that the system is grossly stable for times during which the criteria for containment are met.

THEORY

EQUILIBRIUM RADIAL DENSITY DISTRIBUTION

Assuming a long unbounded cylindrical plasma column with the electrons rotating in synchronism with an applied field

$$B_r = B_o \cos(\omega t - \theta)$$
$$B_\theta = B_o \sin(\omega t - \theta) \quad \ldots (1)$$
$$B_z = B_a$$

Blevin and Thonemann[1] show that

$$j_\theta = -ner\omega \quad \ldots (2)$$

$$B_z(r) = B_a - 2Ne\omega \quad \ldots (3)$$

$$\frac{dN}{dr} = -2\pi nr \quad \ldots (4)$$

where N is the line density of electrons beyond a radius r, i.e. $N = 2\pi \int_r^\infty nrdr$. Introducing the radial equilibrium condition

$$kT \frac{dn}{dr} = j_\theta B_z \quad \ldots (5)$$

they show that

$$N = \frac{B_a}{e\omega}\left[1 - \left(\frac{B_a}{N_o e\omega} - 1\right)\exp\left(\frac{B_a e\omega}{2kT} r^2\right)\right]^{-1} \quad \ldots (6)$$

and derive a radial density distribution

$$n = \frac{B_a^2}{2\pi kT} \frac{\left(\frac{B_a}{N_o e\omega} - 1 \right) \exp\left(\frac{B_a e\omega}{2kT} r^2 \right)}{\left[1 - \left(\frac{B_a}{N_o e\omega} - 1 \right) \exp\left(\frac{B_a e\omega}{2kT} r^2 \right) \right]^2} \qquad \ldots (7)$$

which is valid for a bounded plasma provided the wall density is much lower than the peak density.

EFFECT OF AXIAL FLUX CONSERVATION

We surround the plasma by a cylindrical wall, radius R, which is electrically conducting in the azimuthal direction. Currents will flow in this wall so that axial flux is conserved. The net flux due to electron current in the plasma is

$$8\pi^2 e\omega \int_0^R \left\{ \int_r^R n\, r\, dr \right\} r\, dr \ ,$$

so the wall current must produce a uniform field

$$B_1 = \frac{8\pi e\omega}{R^2} \int_0^R \left\{ \int_r^R n\, r\, dr \right\} r\, dr \qquad \ldots (8)$$

to cancel this flux. Putting

$$N = 2\pi \int_r^R n\, r\, dr \quad \text{and} \quad B^* = B_1 + B_a$$

we find

$$N = \frac{B^*}{e\omega} \left[1 + \left(\frac{B^*}{N_o e\omega} - 1 \right) \exp\left(\frac{B^* e\omega}{2kT} r^2 \right) \right]^{-1} \qquad \ldots (9)$$

Thus the conducting wall has the effect of increasing B_a to a value B^*, which we can show is given by

$$B^* = B_a + \frac{4kT}{e\omega R^2} \ell n \left(\frac{B^*}{B^* - N_o e\omega} \right) \qquad \ldots (10)$$

For constant T the number density is now a maximum at a radius r_o given by

$$r_o^2 = \frac{2kT}{B^* e\omega} \ell n \left(\frac{B^*}{B^* - N_o e\omega} \right) \qquad \ldots (11)$$

which can be expressed

$$r_o^2 = \left(\frac{B^* - B_a}{B^*} \right) \frac{R^2}{2} - \frac{2kT}{B^* e\omega} \ell n \left(\frac{B^*}{N_o e\omega} \right) \qquad \ldots (12)$$

PROPERTIES OF A WELL-DEFINED ANNULUS

The radial density distribution can be expressed in terms of the maximum density $n_o = (B^*)^2/8\pi kT$ as

$$n = n_o \operatorname{sech}^2 [K(r^2 - r_o^2)] \qquad \ldots (13)$$

where $K = B^* e\omega/4kT$. The criterion for a well-defined annulus is taken as $Kr_o^2 \geqslant 2$; since $r_o^2 \approx R^2/2$, this means

$$n_{wall} \approx n_{axis} \approx \frac{n_o}{14} \ .$$

The half-width of the annulus Δr is given by

$$\cosh^2 \left\{ K [(r_o \pm \Delta r)^2 - r_o^2] \right\} = 2$$

i.e.

$$\frac{2\Delta r}{r_o} = \frac{0.88}{Kr_o^2} \qquad \ldots (14)$$

The condition $Kr_o^2 \geqslant 2$ leads to a simple expression for K in terms of the line density N_o, since

$$N_o = \int_0^{R^2} \pi n \, d(r^2) = \frac{\pi n_o}{K} \left\{ \tanh [K(R^2 - r_o^2)] + \tanh [Kr_o^2] \right\}$$

then reduces to

$$K = \frac{2\pi n_o}{N_o} \qquad \ldots (15)$$

From equations (3) and (4)

$$2N_o e\omega = B^* - (B_z)_{r=0}$$

and

$$\frac{dB_z}{d(r^2)} = 2\pi ne\omega \ .$$

Hence

$$K = \frac{2 \left[\frac{dB_z}{d(r^2)} \right]_{max}}{B^* - (B_z)_{r=0}} \qquad \ldots (16)$$

a relation useful for the experimental determination of K.

POWER DISSIPATION AND DECAY OF B_z

The power dissipated as Joule heating per unit length is

$$P = \int_0^R \eta \, j_\theta^2 \, 2\pi \, r \, dr \ .$$

Using equations (2) and (13), and assuming η independent of r , integration gives

$$P = \frac{\eta \, (B^*)^2 \, Kr_o^2}{3\pi} \qquad \ldots (17)$$

The magnetic energy per unit length associated with B_z is

$$W = \int_0^R \frac{B_z^2}{8\pi} 2\pi r \, dr$$

using equations (3), (4) and (13), integration gives

$$W = \frac{(B^*)^2}{8\pi}\left[\pi R^2 - \frac{2\pi}{K}\right] \qquad \ldots (18)$$

The initial decay rate of B_z can be obtained by setting $P = -\frac{dW}{dt}$, which leads to

$$-\frac{1}{B^*}\frac{dB^*}{dt} = \frac{4\eta}{3\pi}\left(\frac{Kr_o^2}{R^2 - \frac{2}{K}}\right) \qquad \ldots (19)$$

a relation which enables η to be estimated from magnetic probe measurements.

CHOICE OF PARAMETERS

The conditions to be satisfied can be expressed as a set of inequalities,

(i) The electrons but not the ions must move with the rotating field

$$\omega_e \gg 2\pi\omega \gg \omega_i \qquad \ldots (20)$$

$$\omega_e \tau_e \gg 1 \gg \omega_i \tau_i \qquad \ldots (21)$$

(ii) The maximum density must occur away from the walls

$$N_o e \omega > B_a \qquad \ldots (22)$$

(iii) The annulus must be well defined

$$Kr_o^2 > 2 \qquad \ldots (23)$$

Assuming a singly ionized plasma, these conditions reduce to

$$\omega_e \gg 2\pi\omega \gg \omega_i \qquad \ldots (24)$$

$$(N_o r_e \omega)^2 \ll \frac{1}{20}\omega_e T^{5/2} \qquad \ldots (25)$$

$$N_o r_e \omega > \omega_{ea} \qquad \ldots (26)$$

$$N_o r_o^2 \omega^2 > 10^{25} T_e \qquad \ldots (27)$$

where r_e is the classical electron radius and ω_{ea} the electron cyclotron frequency in the applied axial field B_a.

Other determining factors are,

(iv) A filling pressure conducive to the production of a well ionized plasma

(v) The limitations of the r.f. system

(vi) The requirement for axial flux conservation

(vii) The reduction of end effects by making the discharge tube long compared with its diameter.

The parameters chosen were

Rotating field : amplitude 200 gauss; angular frequency 8.5×10^6 (1.35 MHz)

Tube dimensions : 100 cm long ; 14 cm diameter

Filling pressure: 0.5 to 5 mtorr.

APPARATUS

GENERAL LAYOUT

The entire apparatus, with the exception of the gas-handling and pumping system, was built in a screened room measuring 21' × 18' × 8' high. This was necessary to minimise electrical interference with the instrumentation, and with neighbouring laboratories.

ROTATING MAGNETIC FIELD

The rotating field was produced by causing suitably-phased r.f. currents to flow in longitudinal conductors situated round the discharge tube. Two pairs of conductors were connected to two identical resonant circuits, accurately tuned to the required frequency of 1.35 MHz and fired in phase quadrature by triggered spark gaps. The r.f. system is described in detail in the Appendix.

In the absence of a plasma the rotating field in the discharge tube had an initial amplitude of 200 gauss and decayed to 40 gauss in 40 μsec.

AXIAL MAGNETIC FIELD

Battery-powered lumped coils provided a steady axial field of up to 600 gauss. The measured uniformity was ± 0.5% over the central 80 cm of the discharge tube, decreasing to -5% at the ends (100 cm apart).

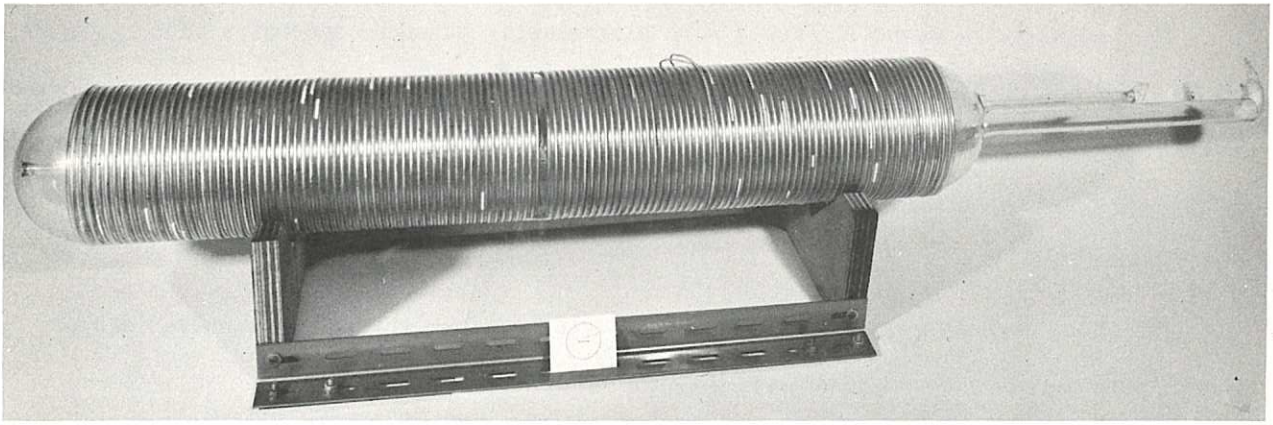

Fig. 3 Discharge tube with flux conserving rings (CLM-R65)

DISCHARGE TUBES

These were made from 14 cm diameter pyrex tube and were 100 cm long (Fig.3). Four types were used,

(i) with axial and radial ports to house magnetic probes,

(ii) with a radial port and a flat end for image converter observations,

(iii) with a radial port and quartz end windows for laser measurements,

(iv) with an open end for connection to a vacuum gauge for pressure calibration.

All discharge tubes were fitted with copper flux-conserving rings of 1/8" minor diameter and spaced 1/8" apart. Their presence reduced the amplitude of the rotating field by $\approx$ 7%. The measured time constant of the flux rings was approximately 0.8 msec, and their efficacy was confirmed by the absence, during a discharge, of any signal from a loop encircling the tube between two flux rings.

PRESSURE MEASUREMENT

An ionization gauge situated in the pumping line outside the screened room was calibrated against a McLeod gauge connected to the end of discharge tube (iv), for both hydrogen and argon.

PRE-IONIZATION

A keep-alive discharge was maintained in the tube by a small 30 MHz oscillator connected symmetrically to two flux rings 60 cm apart, and the main pre-ionization was obtained by the application of a transverse r.f. magnetic field before the main banks were fired. A detailed discussion of the problem of pre-ionization appears in the Appendix.

INSTRUMENTATION

MAGNETIC PROBES

The radial-entry magnetic probes were electrically balanced and had a flat response up to 4 MHz. They could be moved radially and rotated by a remote control mechanism which had a positioning accuracy of 0.5 mm and 1^{o}. The axial-entry probes were housed in slotted metal tubes, which screened the rotating field so effectively that they could be used with one side earthy.

The probe signals were integrated by corrected passive integrators, whose 'droop' characteristic was concave downwards, falling 5% in 50 μsec.

IMAGE CONVERTER

A conventional image converter camera was used to observe argon discharges. To improve perspective, an image-forming system accepting only paraxial light was made. It consisted of focal pair of f/6 lenses, focal lengths 36" and 4", with a small aperture at their common focus.

LASER INTERFEROMETER

The plasma density as a function of radius was measured using a laser interferometer[4]. The low plasma density dictated the use of a multi-pass system, and to obtain radial resolution all the optical paths had to traverse the plasma at the same radius. The mirror system used provided for 16 or 24 passes, and gave a radial resolution of 2 mm at the radius of maximum density.

SPECTROSCOPY

Time-intensity profiles of spectral lines were obtained by using the mirror system of the laser interferometer to transmit light from the plasma to a U.V. monochromator. The narrow aperture of this system ensured that the lines observed originated from that volume element of plasma whose density was being simultaneously measured.

EXPERIMENTAL RESULTS

EFFECT OF FILLING PRESSURE AND APPLIED AXIAL FIELD

Sustained azimuthal currents were observed over pressure ranges of 1.5 – 6.0 mtorr in hydrogen and 0.2 – 2.0 mtorr in argon. At the lower pressures of these ranges, the line density N_o deduced from measurements of B_z corresponded to approximately 10% ionization in hydrogen and to one electron per atom in argon, synchronism being assumed.

Although substantial azimuthal currents could be obtained without the applied axial field B_a, the optimum range was found to be 50 - 100 gauss for both cases. The efficiency of pre-ionization was impaired by reducing B_a to zero.

The experimental results hinge on good shot-to-shot reproducibility. The transient response of the ionization gauge after each shot was found to be very sensitive to variations in filling pressure, pre-ionization conditions and to irregularities in the r.f. supply. Continuous pressure monitoring, using a chart recorder, facilitated good reproducibility and enabled doubtful shots to be rejected.

PLASMA CONFIGURATION DEDUCED FROM MAGNETIC PROBE MEASUREMENTS

The radial distribution of the azimuthal currents in the plasma was measured in two ways: (i) by measuring $B_z(r)$ with a single movable probe, plotting B_z against (r^2) and then differentiating (Fig.4); (ii) by measuring $\frac{dB_z}{dt}$ directly, using a differential probe consisting of two identical coils spaced 1 cm apart, and plotting $\frac{1}{r}\frac{dB_z}{dr}$ against r. The radial density distribution was then inferred on the assumption of synchronism with the rotating field.

These measurements were made using the radial probe port at the centre of the tube, and confirmed the existence of an annular plasma there. That the annular configuration extended over the length of the tube was confirmed as follows. Measurements of $(B_z)_{r=0}$ as a function of z were made using the axial probe port and extending beyond the end of the tube. Then the axial field of a solenoid of radius 5 cm ($\sim r_o$) and 100 cm long, carrying an r.f. current, and enclosed in a conducting tube of radius R, was also measured.

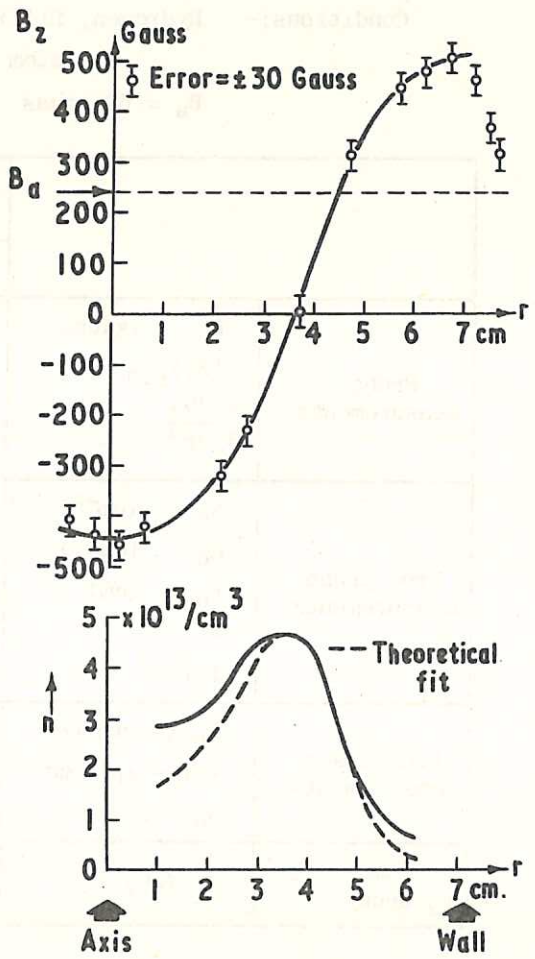

Fig. 4 Experimental conditions with 0.95 mtorr argon (CLM-R65)

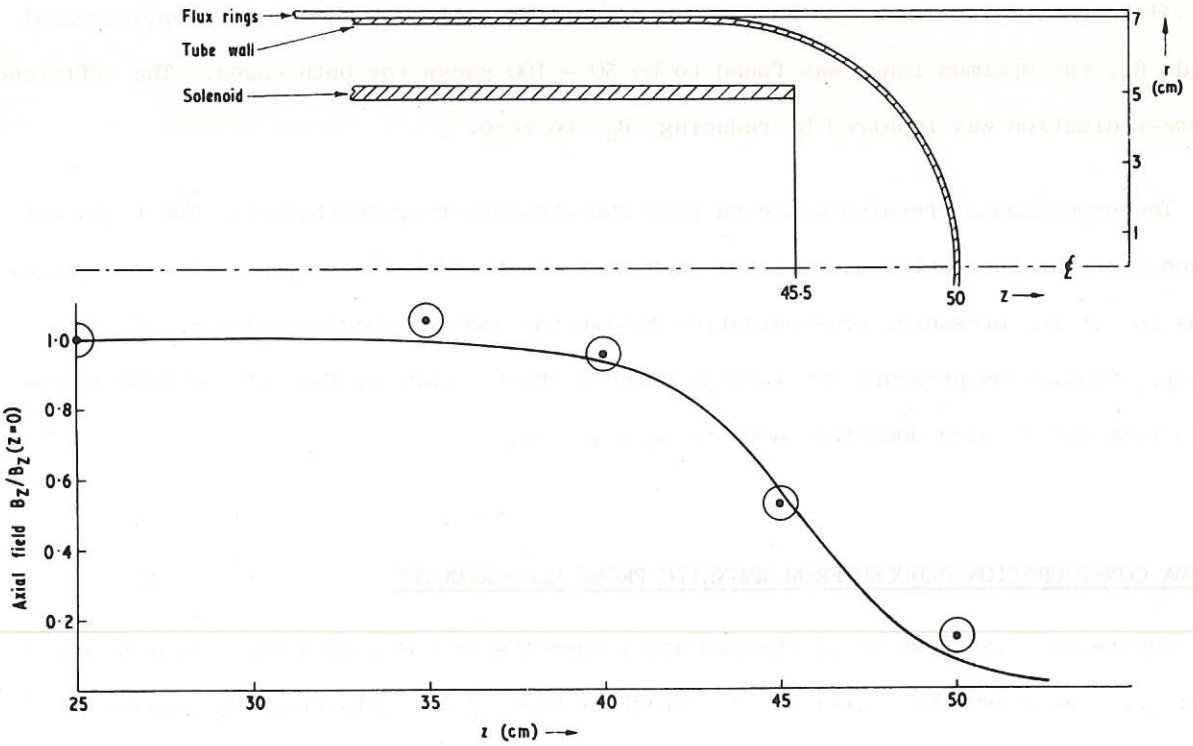

Fig. 5 (CLM-R 65)

Z dependence of axial field. Solid curve : B_z of solenoid located as shown above.
Points : B_z of annular plasma

TABLE 1

Conditions:- Hydrogen, filling pressure: 1.0 mtorr

atom line density : 1.1×10^{16} cm^{-1}

B_a = 60 gauss

		Time after firing (μsec)		
		11	15	19
Probe measurements	B^* (gauss)	310	285	270
	$(B_z)_{r=0}$	-330	-285	-255
	$\left(\frac{dB_z}{dr^2}\right)_{max}$	30	30	35
From probe measurements	N_o (cm^{-1})	$2.4(10)^{15}$	$2.1(10)^{15}$	$1.9(10)^{15}$
	n_o (cm^{-3})	$3.5(10)^{13}$	$3.5(10)^{13}$	$4.0(10)^{13}$
	r_o (cm)	5	6	5
	K	0.10	0.10	0.12
	T (eV)	70	57	43
From laser measurements	N_o (corrected for slip)(cm^{-1})	$2.6(10)^{15}$	$3.6(10)^{15}$	$3.6(10)^{15}$
	n_o (cm^{-3})	$3.8(10)^{13}$	$6.0(10)^{13}$	$7.6(10)^{13}$
From B_z decay	T_e (eV)	-	-	15

Comparison of the decrease in B_z with z in the two cases was consistent with the annular plasma extending the full length of the discharge tube (Fig.5).

Analysis of the magnetic probe measurements indicate three distinct phases:

(i) Ionization phase (discussed in the Appendix). The line density builds up and the annular structure forms.

(ii) Annular phase. A well-defined annular structure is observed, with a radius in good agreement with equation (12). From the width of this annulus the parameter K can be evaluated, either graphically or by the use of equation (16). The value of plasma temperature obtained from K, as will be seen in Table I, is larger than that obtained by other methods. Under conditions when this phase is prolonged, the radius of maximum density r_o is observed to oscillate slowly, moving first inwards, then outwards, with a period of about 20 μsec (Fig.6).

(iii) Decay phase. The annular phase is terminated by the abrupt exclusion of the rotating field from the plasma, and the azimuthal currents decay with a time constant of 10–20 μsec. By measuring the initial decay rates of B_z and using equation (19), plasma resistivities of the order of 10^7 e.m.u. are obtained, which are consistent with the value of $\omega_e\tau_e$ ($= B_o/ne\eta$) approaching unity.

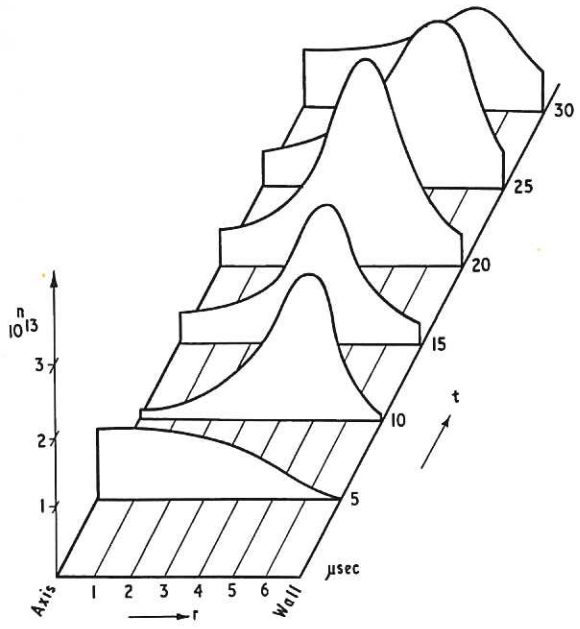

Fig. 6 (CLM- R 65)
Temporal variation of radial density
Argon, p = 0.9 mtorr, $B_a = 0$

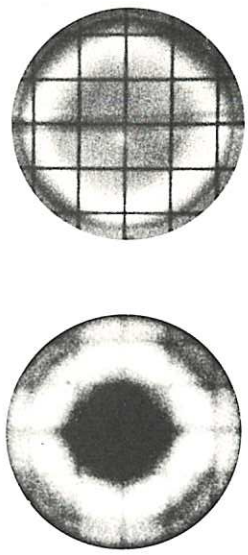

Fig. 7 (CLM- R 65)
Image converter photographs of argon plasma:
upper - focal lens system, 6 μsec exposure,
lower - single objective, 1 μsec exposure
(grid is 1 inch square)

IMAGE CONVERTER OBSERVATIONS

Photographs of discharges in argon, taken with the image converter, demonstrated the annular shape of the plasma (Fig.7). The luminous zone appeared to be ~ 5 cm radius and ~ 2 cm thick. Radial movement of the annulus could not be resolved; the small aperture

of the focal lens system made exposure times of 15-25 μsec necessary, while perspective effects obscured any movement when a single objective was in use.

A slight barrel distortion of the annulus was evident, and was attributed to non-uniformity of the rotating field.

DENSITY MEASUREMENTS USING A LASER INTERFEROMETER

Measurements of the mean electron density over the length of the tube were made at radii of 3, 4, 5 and 6 cm. A sixteen-pass mirror system[2] was found to be the best compromise between sensitivity and experimental convenience; the density change corresponding to one fringe was $4 \times 10^{13} cm^{-3}$. Density-time profiles were derived graphically by finding the best fit to the data from several interferograms, selected with different initial phasing. In this way the accuracy was increased to an estimated ¼ fringe ($1 \times 10^{13} cm^{-3}$). Radial density distributions derived from these profiles were less accurate, since they depended on the long-term reproducibility of the discharge (the interferometer had to be re-aligned after each radial movement).

The peak densities measured during the annular phase exceeded those derived from probe measurements, indicating slip between the electrons and the rotating field. In a typical case the slip would increase from ~10% to ~40% during the annular phase.

Taking finite resistivity into account, equation (2) for the azimuthal current density becomes

$$j_\theta = - \frac{ner\omega}{1 + \frac{2}{(\omega_e \tau_e)^2}} \qquad \ldots (28)$$

The observed slip would thus be expected as the value of $\omega_e \tau_e$ approaches unity.

SPECTROSCOPIC OBSERVATIONS

Integrated spectrograms of argon discharges were obtained with the medium quartz spectrograph. All the lines identified arose from argon ions, with the faint exception of C III (2296). Suitable lines from A II, A III and A IV were chosen and their time-intensity profiles recorded with the U.V. monochromator set at the radius of maximum density. The method of Hobbs and Rose[5] of obtaining the electron temperature from these profiles gave contradictory results from the different ionic species, presumably due to the injection of ions from adjacent radii.

A rough estimate of the electron temperature was deduced from the observation that the initial peak of A III lines occurred between 4.5 and 12 μsec after firing, for electron

densities in the range 5 to 10×10^{13} cm^{-3}. Calculated ionization probabilities of A II for $n_e = 10^{14}$ cm^{-3} are

$3/2\ kT_e$	10	20	40	60	eV
$\frac{1}{n_e\ (Qv)}$	1060	33	4.9	2.5	μsec

which suggest kT_e is in the range 20 to 30 eV.

Some of the A IV profiles observed at a radius of 5 cm exhibited slow fluctuations, corresponding to the oscillation of the annular radius detected by magnetic probes.

CONCLUSIONS

The formation of an annular cylindrical plasma, contained by the solenoid magnetic field of azimuthal electron currents induced in it, has been demonstrated by three independent methods. Theoretical predictions and experimental observations of the properties of the annular plasma are in fair quantitative agreement, with one exception; the temperature deduced from radial pressure balance is higher than that inferred from spectroscopic observations and field diffusion times. A similar discrepancy was found by Blevin and Thonemann[1], who attributed it to complications arising from end effects. Their explanation is applicable to our results, since in both cases the discharge tubes used had similar ratios of length to diameter.

The lifetime of the annular plasma reached about 40 μsec at the lowest operating pressures. It appeared to be limited by the decay of the rotating field, which caused $\omega_e \tau_e$ to approach unity, rather than by the onset of any gross instability.

ACKNOWLEDGEMENTS

The authors express their gratitude to Drs. H.A. Blevin and P.C. Thonemann for helpful discussions and to Messrs. S.G.F. Blewett and N.H. Price, who rendered valuable assistance with the instrumentation.

REFERENCES

1. BLEVIN, H. and THONEMANN, P.C. Plasma confinement using rotating magnetic fields CLM-R 12 H.M.S.O., 1961. Also in Nucl. Fusion 1962 Supplement, Part I, p.55.

2. DAVENPORT, P.A., FRANCIS, G. and MILLAR, W. Plasma confinement using a rotating magnetic field (Abstract only). Bull. Amer. Phys. Soc., series 2, vol.9, no.3, p.355, 1964.

3. DAVENPORT, P.A. D. Phil Thesis, Oxford University 1954.

4. TAYLOR, A.F. Culham Laboratory, Unpublished information, 1965.

5. HOBBS, G.D. and ROSE, M.A. The life history of impurity atoms in a plasma possessing a time varying electron temperature and density. CLM-R 3 H.M.S.O., 1963.

6. WHIPPLE, R.T.P. A screening problem with application to the thetatron. A.E.R.E. - R 3305 H.M.S.O., 1960.

APPENDIX: The r.f. system

1. GENERAL DESCRIPTION
2. THE INDUCTIVE COMPONENTS
3. THE CAPACITOR BANKS
4. SPARK GAPS AND TRIGGERING SYSTEM
5. THE NEED FOR PRE-IONIZATION
6. PRE-IONIZATION THEORY
7. THE PRE-IONIZATION CIRCUIT
8. WAVEFORM MONITORING AND CIRCUIT MEASUREMENT

APPENDIX

1. GENERAL DESCRIPTION

The rotating magnetic field is set up by two fixed loops as shown in Fig.8; each loop carries a sinusoidal current of the same frequency (1.35 MHz) and amplitude (14 kA), but there is a phase difference of 90^{o} between the two currents. The loops are driven by a simple oscillatory circuit containing inductance, capacity and spark gaps in series; the oscillations decay to half amplitude in 40 or more cycles, with a discharge present. The initial value of the rotating field on the axis is 200 gauss. In the first half or so of the pulse the losses are chiefly due to ohmic heating in the metallic parts of the circuit, giving an exponential decay; in the later stages the arc drop in the spark gaps is the dominant loss, giving a linear decay envelope which reaches zero amplitude after about 100 cycles, when the capacitor voltage has become so low as to be unable to overcome the arc drop in the switches. The phase difference is obtained by firing the spark gaps in one circuit a quarter period or 185 nsec later than those in the other. The inductance of each loop is 420 nH and so with the above current and frequency the voltages across the ends are each 50 kV.

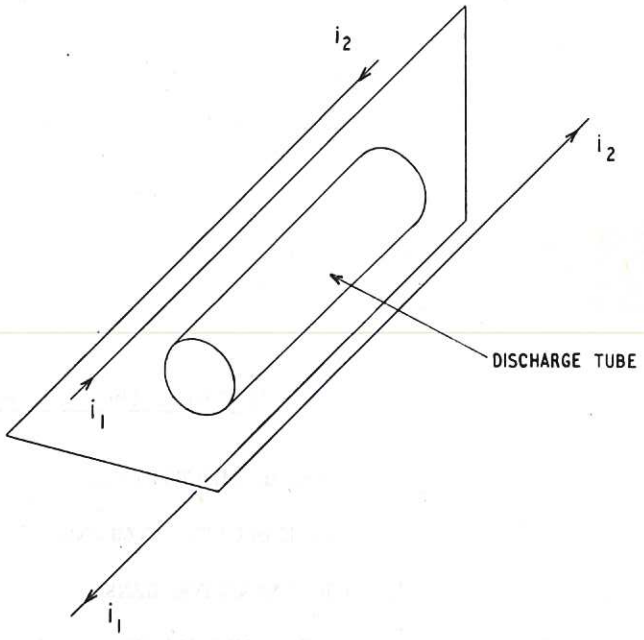

Fig. 8 The two fixed loops for rotating magnetic field (CLM-R65)

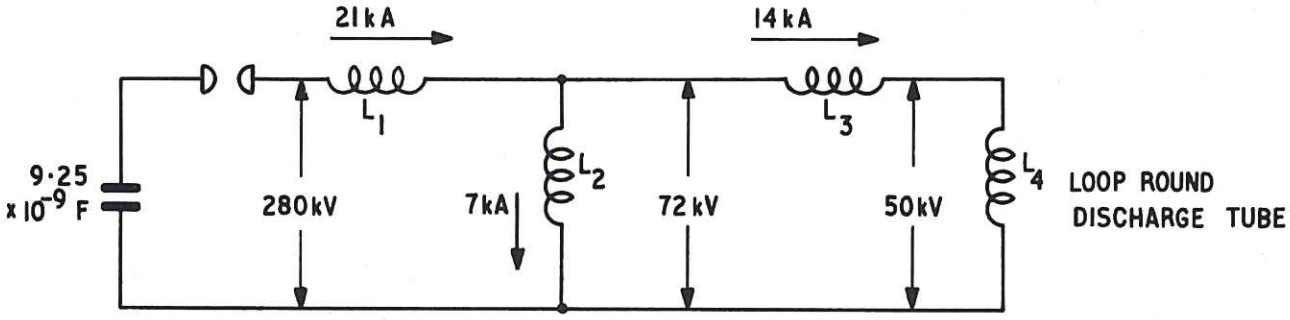

Fig. 9 Basic circuit diagram for each of the two driving loops (CLM-R65)

The magnetic energy in each loop is 42 joules. In order to achieve a large number of cycles of damped oscillation, the total stored capacitor energy is an order of magnitude greater; some of this stored energy is slowly dissipated as conductor loss in the loop, and in power conveyed to the discharge. The extra stored energy requires that there be considerable inductive storage outside the main loop, achieved by means of a circuit whose principle features are shown in Fig.9. The inductance values and their

associated energies are:

L_1	1110 nH	250 joules	L_3	180 nH	18 joules
L_2	1200 nH	30 joules	L_4	420 nH	42 joules

The total energy per phase is thus 340 joules. The corresponding currents and voltages are shown in the figure. In practice four capacitors and switches are used in series, because of the high voltage; a part of L_1 is assigned to each capacitor, so that no unduly high electric fields are produced.

2. THE INDUCTIVE COMPONENTS

Each driving loop, L_4, consists of three copper tubes, electrically in parallel, with part of the circuit consisting of a thick copper end-plate as shown in Fig.10. The whole assembly is enclosed by a thick aluminium shell which prevents coupling between the driving loops and external components such as the D.C. field coils. Note that the two loops are fed from opposite ends of the discharge tube. A scale drawing of a section through the device, normal to the axis, is given in Fig.11. The proportions shown result in a satisfactory degree of uniformity of rotating field within the area of the discharge tube. Each end-plate is in contact with the outer shell, and has a pair of openings to allow one set of conductors to pass through. The edges of these openings are rounded off to reduce electrical stresses.

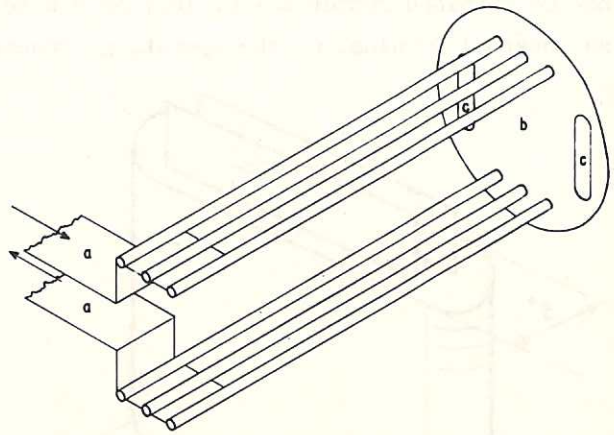

a TRANSMISSION LINE
b END PLATE
c OPENING FOR CONDUCTORS OF OTHER LOOP

Fig. 10 (CLM-R65)
Construction of one driving loop for rotating magnetic field

The inductance L_3 in Fig.9 consists of an air-insulated strip transmission line, which forms part of the connection between the capacitor bank and the loop. The transmission line is made of copper sheets, 35 cm wide and 10 cm apart, with curved edges of 2.5 cm radius. The ends of the six tubes forming one driving loop project beyond the end plates and act as supports for the transmission line to which they are connected.

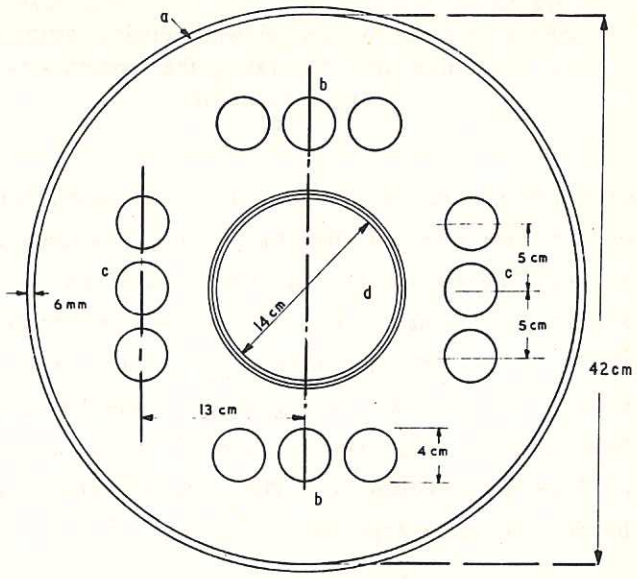

a. ALUMINIUM SHELL
b. FIRST DRIVING LOOP
c. SECOND DRIVING LOOP
d. DISCHARGE TUBE

Fig. 11 Section of the conductor assembly (CLM-R65)

The inductance L_2 is a two turn loose helix of copper tubing, connected across the strip transmission line. The inductance L_1 is variable, giving a frequency range of a few percent, and is part of the capacitor bank system, described in the next section.

3. THE CAPACITOR BANKS

The capacitors for the oscillating circuit were made in the laboratory, because of the requirement for low loss at high voltage. It is probable that suitable capacitors could now be obtained commercially. They have a self-resonant frequency in excess of 10 MHz and an internal Q value, at the operating frequency of 1.35 MHz, in the region of 1000, which is consistent with calculated conductor losses inside the capacitor. In a resonant test circuit, overall Q values (including losses in the tuning inductance) of 400 have been measured at low amplitude; tests in high-voltage ringing circuits with corrections for the spark gaps have shown that no additional losses are present in the capacitor at full voltage. The operating Q in the complete system, measured at low voltage and with the spark gaps short-circuited, was about 250; thus in free oscillation the current decayed by a factor 1/e in about 80 cycles. The capacitors have electrodes of thick aluminium foil, with insulation of polythene immersed in medicinal liquid paraffin. They are made in units of 0.075 μF at 40 kV, each consisting of two 20 kV parts in series, with the centre tap connected to the container. The 40 kV unit is immersed in paraffin in a copper can, open to the atmosphere; no deterioration has been observed over a period of years. The terminals take the form of two wide strips protruding from the top as shown in Fig.12. As a number of units have to be connected in series, there is an r.f. electric field on the outside of the cans, which are therefore made with rounded edges where possible. In use, the cans rest in a shallow tray of oil which covers the sharp lower edges. Several units were tested with 10^4 shots in a high Q ringing circuit at 40 kV, and showed no loss of performance. The working voltage in the experiment was restricted to 35 kV because of the spark gaps.

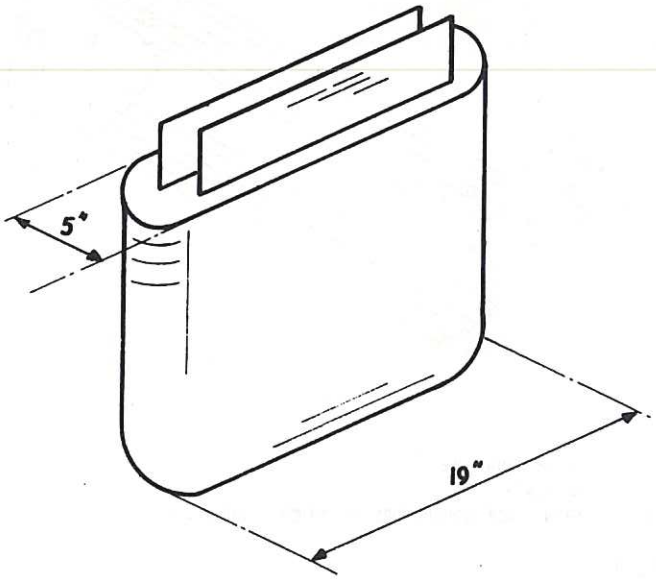

Fig. 12 (CLM-R65)
Sketch of capacitor can, showing terminal strips. An insulating strip separating the terminals is omitted for clarity

A sketch of one complete capacitor bank is shown in Fig.13. There are two such banks in the complete system, one per phase. Fig.14 is a circuit diagram, in which each heavy capacitor symbol represents one can unit. The inductance L_1 is formed by the loop

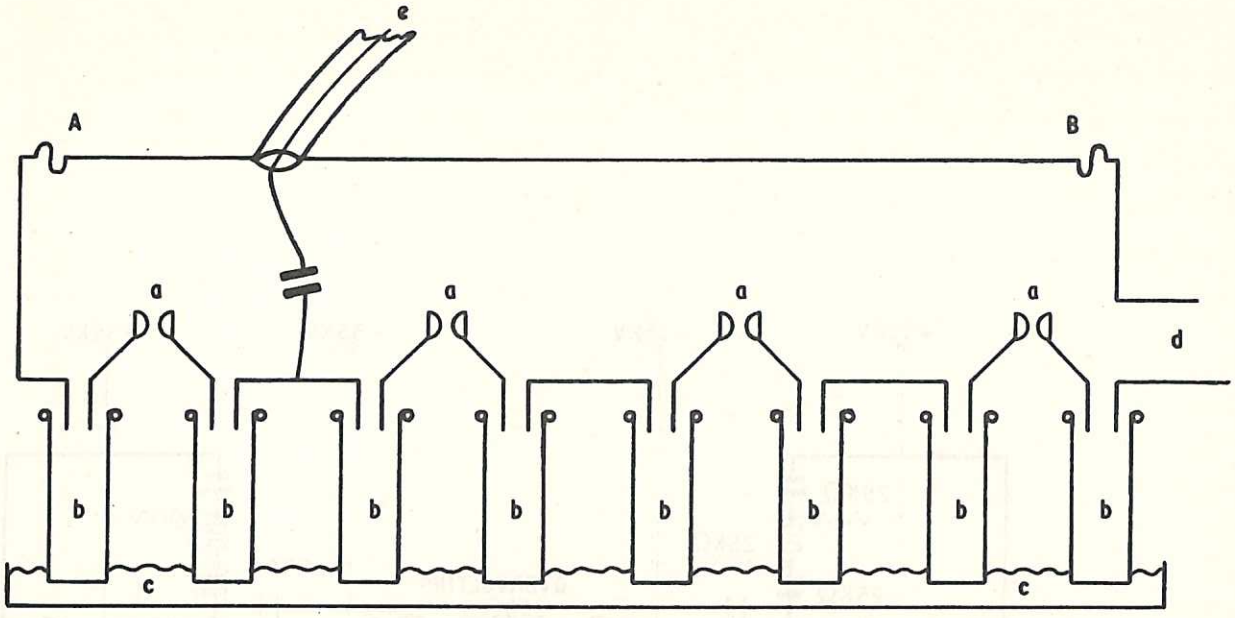

a. SPARK GAPS
b. CAPACITOR CANS
c. OIL TRAY
d. TRANSMISSION LINE
e. OVERVOLTING CABLE

Fig. 13 Sketch of one complete capacitor bank (CLM-R65)

consisting of the capacitor terminals, the leads to the spark gap switches, and the copper strip AB in Fig.13. Some inductance is of course associated with the capacitor elements and with the arc channels in the switches. The strip AB can be raised and lowered for tuning.

4. THE SPARK GAP SWITCHES AND TRIGGERING SYSTEMS

Switching in the above circuit is a difficult problem which has not been completely solved; the present spark gaps operate satisfactorily when holding off 70 kV, but not 80 kV. Even at 70 kV the gaps have to be taken apart frequently for cleaning. The requirements of the switch are as follows:

(i) In a ringing circuit the resistive voltage, or arc drop, across a spark gap is of approximately constant magnitude, E, alternating in sign so as always to oppose the current. Simple analysis then shows that the peak capacitor voltage diminishes by 4E per cycle due to the arc loss alone. Thus we must keep the arc loss as low as possible, so pressurisation is used. If intermediate electrodes are used for triggering, the number of arcs in series is doubled and the total arc drop is almost doubled.

(ii) The r.f. resistance of the connections must be low. At a frequency of 1 MHz, skin effect raises the resistance of even pure cold copper to about ¼ mΩ in a region of high current convergence such as an arc root; there is a logarithmic dependence on the convergence ratio which therefore hardly affects the resistance.

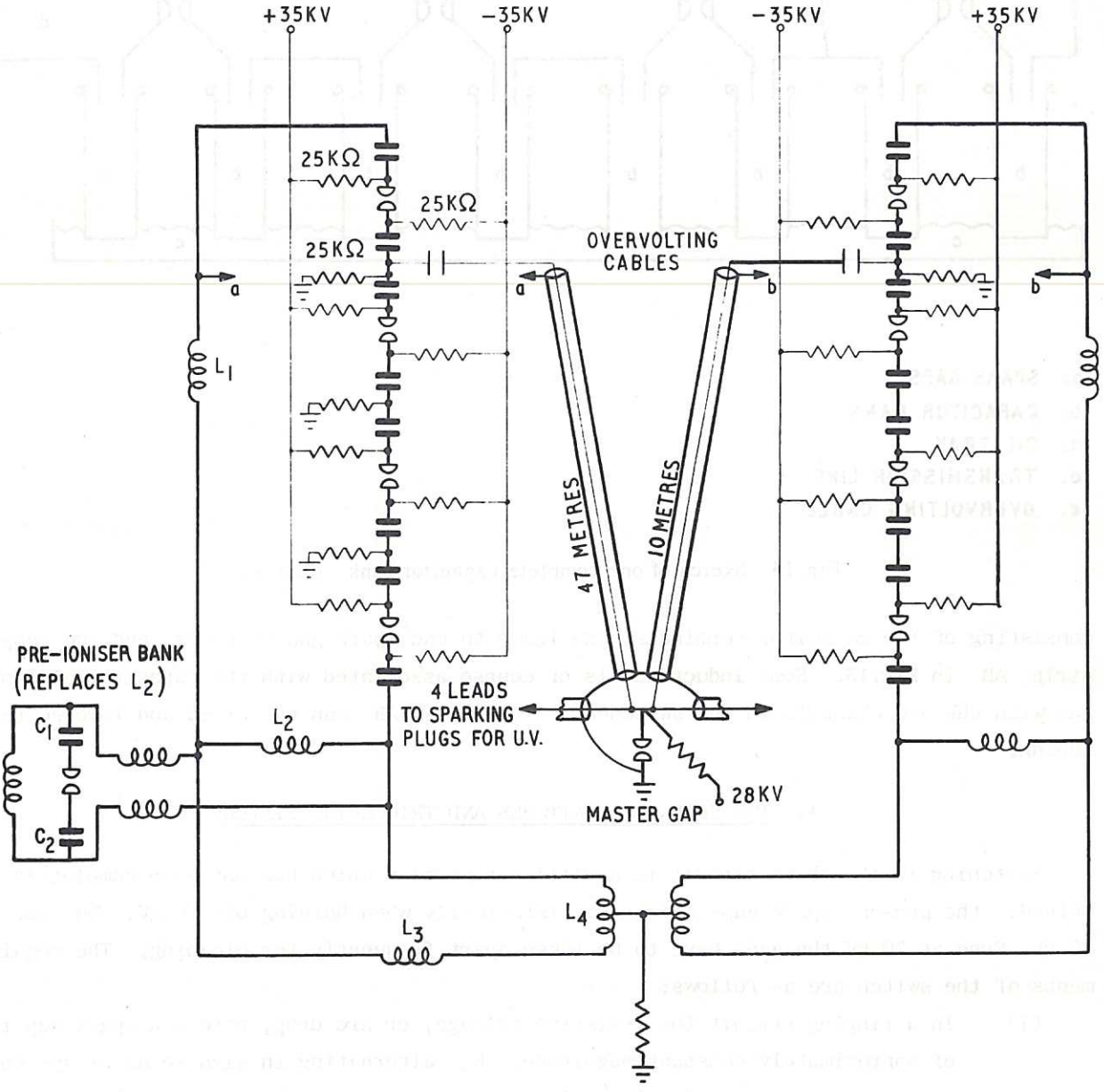

Fig. 14 (CLM-R65)
Circuit diagram with charging and triggering systems.
The R.F. circuits are shown in heavy lines

(iii) All four gaps in one bank must fire within a certain time interval (~ 100 nsec), otherwise very high transient voltages appear, causing external breakdown. The permissible interval is determined by stray reactance in the assembly.

(iv) The main r.f. circuit is not complete until all four gaps have fired; the time at which the last gap fires determines the phase of the resulting oscillations. The requirements of the rotating field demand relative timing accuracy between the completion of the two circuits of 10 nsec or better.

(v) The time-average of the modulus of the arc current over the ringing period of 50 μsec is ~ 10^4 A and hence the electrodes experience erosion equivalent to the passage of 0.5 coulomb.

Because of the above requirements, the switches are of a simple and rugged construction, using semi-spherical copper electrodes enclosed in pressurised plastic cases with copper end-plates. Triggering is carried out by firstly illuminating the negative electrode with pulsed ultra-violet light from a remote auxiliary arc, and then rapidly overvolting the gap by a factor ~ 2. It is sufficient to apply a special overvolting signal to only one of the gaps, but all four must be illuminated. Breakdown of the first gap then causes successive overvolting and breakdown of the others, as in the Marx generator.

All eight spark gaps in the system are identical; a section of one is shown in Fig.15. The ultra-violet light comes from a suitable car sparking plug. The P.V.C. tubes in which the plugs are mounted have an internal polish which helps to concentrate the light. Carbon dioxide is satisfactory as an insulating gas, at pressures of up to 5 atmospheres. The resulting force on the copper end-plates is carried by the six short nylon studs. If a sparking plug fails to fire for any reason, a very high voltage builds up, especially across the last gap. It is deliberately arranged that if this happens, flash-over takes place on the outside rather than the inside of the plastic shell.

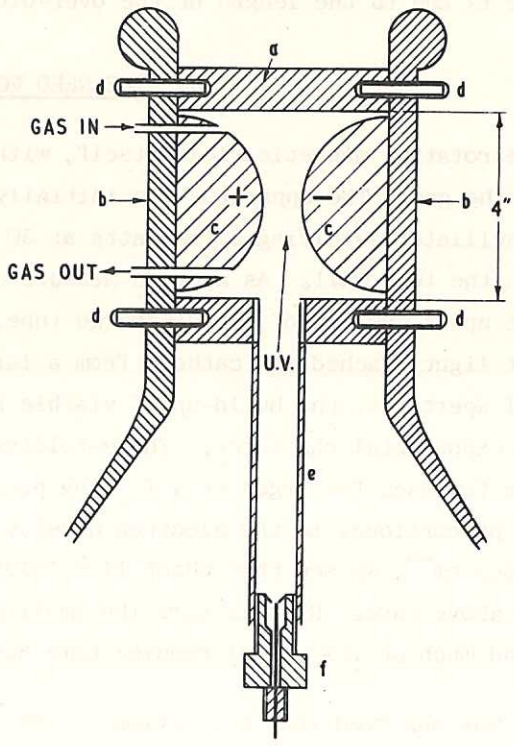

a. P.V.C. PRESSURE VESSEL.
b. COPPER END PLATES.
c. HEMISPHERICAL COPPER ELECTRODES.
d. NYLON STUDS, 6 EACH END.
e. P.V.C. TUBE.
f. SPARKING PLUG.

Fig. 15 Section of a spark gap (CLM-R65)

The triggering circuit is shown in Fig.14. The master gap is of conventional design with radial insulation, and can be triggered either by reducing the gas pressure or by applying a voltage pulse to a trigger pin. The rise time of the voltage pulses in all output cables is of order 20 nsec, and is determined by the time-constant L/R where L is the master-gap inductance and R is the impedance of the output cables in parallel. The

interval of 185 nsec between the closure of the two circuits is achieved by having one overvolting cable 37 metres longer than the other. The rate of rise of overvoltage across the first gap is smaller than in the cable, due to stray reactances in the intervening circuit. The total swing of the overvolting signal, at the open end of the cable is twice the master gap voltage, or 56 kV; at the first gap the available swing is greater than this, again due to stray reactance. The method of connecting the overvolting cable is shown in Fig.13. By adjusting the position of the lead, the oscillatory (1.35 MHz) voltage fed back into the cable after all the gaps have fired can be reduced almost to zero. It is also necessary to avoid the flow of large H.F. currents in the outer braid of the cable; that is achieved by routing the cable through one of the tubes comprising the rotating field loop. Some of the sparking plug cables were routed in the same manner, to avoid flash-over along the plug supports.

It is not very easy to measure the time at which each main gap fires. However, the phase of the high frequency currents in each driving loop can be monitored accurately as described in section 6. Provided the main gaps are in clean condition, reliable triggering is obtained and the timing error between the two banks seldom exceeds 7 nsec, which is adequate for the generation of the rotating field. The time elapsing between the firing of the master gap and the firing of the final gap in the first bank is 150 nsec, of which 50 nsec is due to the length of the overvolting cable.

5. THE NEED FOR PRE-IONIZATION

The rotating magnetic field itself, with its associated electric field, may be used to ionize the gas. The apparatus was initially so operated, with the addition of a keep-alive C.W. oscillator supplying a few watts at 30 MHz to the discharge by capacitive coupling through the tube wall. As a crude measure of the rate of ionization, a diffusing screen was set up at one end of the discharge tube. A photo-multiplier was exposed to the screen so that light reached its cathode from a large part of the discharge. Using a range of optical apertures, the build-up of visible radiation was observed over many decades and had an exponential character. The e-folding time varied inversely as the filling pressure, being a few μsec for argon at a filling pressure of 1 mtorr. Assuming that the light output is proportional to the electron density, and that the C.W. oscillator produces 10^8 electrons cm^{-3}, we see that about 14 e-foldings are required, requiring some tens of μsec in the above case. By this time the amplitude of the rotating field has decayed considerably and much of its useful running time has been lost.

It was observed that excitation of one loop was as effective for ionization as of both. It was therefore decided to pre-ionize by using an auxiliary capacitor bank to excite one loop before the application of the rotating field. An analysis of the situation (section 6) indicated favourable values of field, frequency and duration. A circuit was then designed (section 7) which fulfilled these requirements without affecting the rotating field.

6. PRE-IONIZATION THEORY

Take co-ordinates z along the tube axis, and y parallel to the r.f. magnetic field B_y, with $x=y=o$ on the axis and $z=o$ at one end of the tube. If

$$B_y = B_o \sin \omega t, \qquad \ldots (A1)$$

then we have for the electric field

$$\frac{\partial E_x}{\partial z} - \frac{\partial E_z}{\partial x} = -\frac{1}{c}\,\omega B_o \cos \omega t \ . \qquad \ldots (A2)$$

In vacuo the E_z component vanishes, the field E_x terminating in charges on the surface of the conducting loop. A very weak plasma is sufficient to screen out these charges, giving

$$E_x = 0$$

$$E_z = (\omega B_o\, x/c) \cos \omega t. \qquad \ldots (A3)$$

The flux-conserving rings have a similar screening effect, treated by Whipple[6]. The fact that E is now parallel to the D.C. magnetic field B_a favours ionization. Consider an electron at rest at t=o, z=o, $x=x_1 < R$. With $B_a \gg B_o$, and x and y motions are small and we have for the z motion using equation (A3),

$$\partial^2 z/\partial t^2 = -\,\omega\,\omega_{ea}\, x_1 \cos \omega t, \qquad \ldots (A4)$$

which with the above initial conditions can be integrated to give for the electron energy W,

$$W = \frac{1}{2}\, m\, x_1^2\, \omega_{ea}{}^2 \sin^2 \omega t \qquad \ldots (A5)$$

provided the electron does not reach the far end of the discharge tube. Taking the tube length as 100 cm, and a typical value x_1 of 5 cm, equation (A5) yields for the maximum energy W* in electron-volts,

$$W^* = B_o^2/5, \quad B_o \ll 100 \text{ gauss} \qquad \ldots (A6)$$

For $B_o > 100$ gauss the electron hits the far end of the tube and W* increases with B_o less rapidly than in equation (A6). When B_a is small the x motion is important, and electrons strike the side walls with energies again less than given by equation (A6).

Since the optimum energy for ionization is usually in the range 100–1000 eV, we see that B_o should lie in the range 20–60 gauss. It was found experimentally that, with B_o initially 40 gauss, ionization was three times more rapid than with a B_o of 200 gauss.

We can obtain a lower limit to the ionization e-folding time, T_{min}, in argon by assuming all electrons to have energies in the vicinity of 100 eV. For a neutral gas pressure of p mtorr, the ionization mean free path in argon, λ_e, is then given by

$$\lambda_e \approx 100/p \text{ cm}$$

and is therefore less than or comparable with the tube length at all pressures of interest. Further, since

$$T_{min} \approx \lambda_e/u$$

where u is the velocity corresponding to 100 eV, or $6 \cdot 10^8$ cm sec^{-1}, we have

$$T_{min} \approx 10^{-7}/p \text{ sec}$$

In practice the e-folding time is one or two orders of magnitude greater than this, because of electron energy spread and charged particle loss.

7. THE PRE-IONIZATION CIRCUIT

The function of the circuit is to supply one of the driving loops with an oscillatory current waveform whose envelope is shown in Fig.16. The relevant circuit is shown in Fig.14; it replaces the inductor L_2. The capacitor C_1 and C_2 are each one can unit, identical to the sixteen others in the main banks. The inductors are chosen to fill the two conditions:

(i) The initial B_o is 30 gauss

(ii) The impedance looking in at the terminals with the spark gap shorted out is the same as that of the inductor L_2 which the new network replaces.

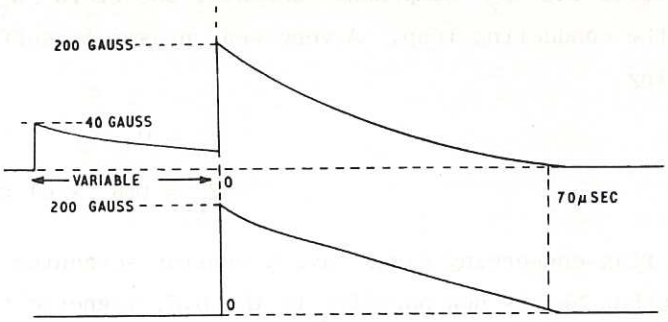

Fig. 16 (CLM-R65)
Envelopes of the R.F. magnetic field contributions of the two loops, with the pre-ionizer connected to one loop only

When the inductors were so chosen it was found that the pre-ionizer ringing frequency was 1.5 MHz; the performance of the main bank was not affected. The pre-ionizer was fired by reducing the gas pressure in the gap; the main banks were triggered from it by means of a pick-up loop, a variable delay unit, and a 15 kV thyratron which pulsed the trigger pin on the master gap. When the delay was set to less than the duration of the pre-ionizer pulse, beats were observed in the loop current; the beats disappeared when the master gap was fired at a certain phase with respect to the pre-ionizer oscillations, and so a synchronised delay with phase control was introduced. The pre-ionizing device enabled the useful filling pressure to be lowered by a factor of five.

8. WAVEFORM MONITORING AND CIRCUIT MEASUREMENTS

8.1 The Rotating Field

The current waveforms in the two driving loops are monitored by two single-turn unbalanced coils mounted close to the end plates where the electric field is low, and each one is so orientated that it responds only to that rotating field loop which terminates there. A calibration coil of known area, positioned symmetrically about and midway along the tube axis, is orientated to couple equally to the two driving loops. Because it is in a region of high electric field it is used with balanced connections. Once the ratio between its output and that of the monitor coils has been established, it is removed from the apparatus. The signals are operated upon by an R-C integrating network; the resulting waveforms depict the two components of the rotating magnetic field, whose absolute amplitude is known from the calibrating ratio.

The following method is used to display the quality of the rotating field. A sufficient criterion is that the amplitudes of the separate components due to the two driving loops be equal in frequency and amplitude, and different in phase by 90^o. Because of the large number of cycles in the pulse, it is not practicable to observe the phase difference directly at all times. However, if we denote the two components by vectors $\underline{A}$ and $\underline{B}$, then, under conditions of correct amplitude adjustment where $|\underline{A}| = |\underline{B}|$, the phase

difference φ is given by

$$\tan(\varphi/2) = |\underline{A}+\underline{B}|/|\underline{A}-\underline{B}|$$

The "B" monitor loop is duplicated in reverse, so that signals representing both $\underline{B}$ and $-\underline{B}$ are available. The sum signals $(\underline{A}+\underline{B})$ and $(\underline{A}-\underline{B})$ are formed in the integrating networks as shown in Fig.17; slight inequalities in the three monitor loops are corrected by adjustment of the resistors in the network. The two sum signals are presented separately on a double-beam oscilloscope, when the ratio of the moduli at any instant may readily be estimated. Fig.18 shows three such pairs of oscillograms; in the first pair there is a frequency error and beats are apparent, in the second there is a phase error, and the third indicates a good rotating field. An occasional check on the ratio $|A|/|B|$ is necessary; if for example one bank does not fire at all, the above display would still appear to show a perfect rotating wave. The cables to the oscilloscope are fed through the wall of the screened room using bulkhead connectors, so that spurious signals do not travel on the outsides of the cables.

8.2. Circuit Parameters

It is important to measure the inductances L_1 to L_4 in Fig.9, and also the losses in various parts of the system. Most of the loss occurs in the copper parts constituting these inductances, but additional losses can occur in many ways, and it was necessary to track down and remedy a large number of small effects each quite small in itself. For example poor joints, coupling to the overvolting cables, or large masses of iron inadvertently left near the circuit all cause losses at low amplitude; excessive corona discharges and faulty capacitors show losses only under high voltage operation. For the low voltage tests the spark gap electrodes are clamped together,

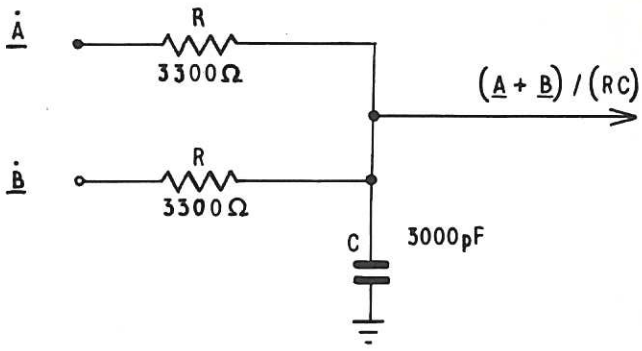

Fig. 17 (CLM-R 65)
Network for addition and integration of signals

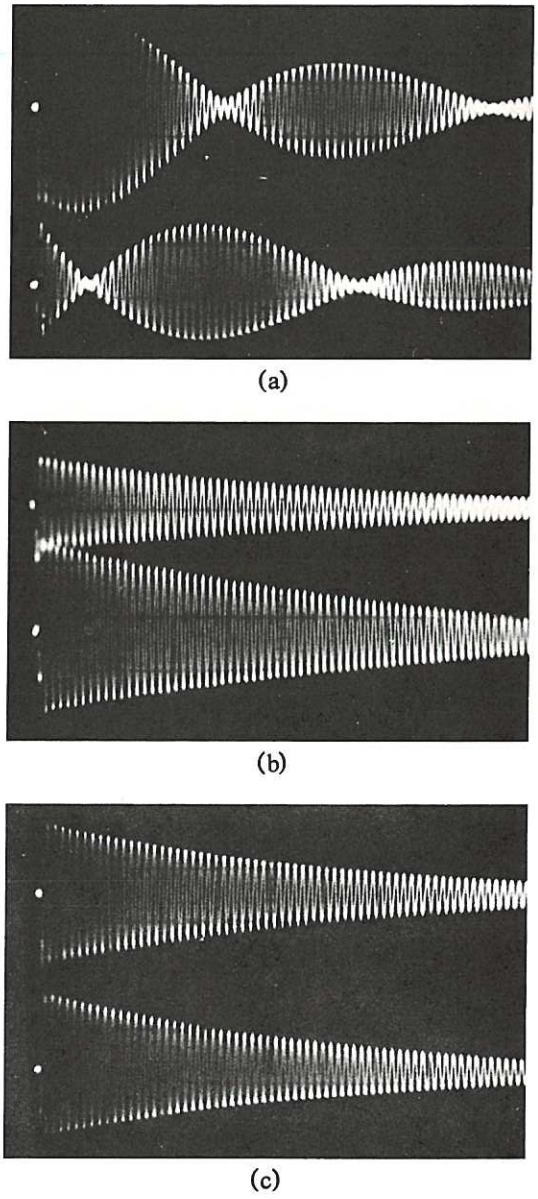

Fig. 18 (CLM-R 65)
Monitoring the rotating field: (a) frequency error; (b) phase error; (c) good adjustment

and the circuit is excited by inductive coupling to a signal generator with a calibrated attenuator. The excited amplitude is measured with a high-frequency voltmeter, also inductively coupled. Keeping the voltmeter reading constant, the signal generator output v is noted at various frequencies f. Because the circuit exhibits a simple resonance we have

$$(v/v_0)^2 = 1 + 4Q^2 (1 - f/f_0)^2$$

where v_0 is the minimum input voltage and f_0 is the resonant frequency. A plot of $[v/v_0)^2 - 1]^{\frac{1}{2}}$ against f should yield a straight line intercepting the axis in f_0 and having a slope $2Q/f_0$. In this way f_0 and Q can be measured accurately. For the inductance L_1 to L_4, the frequency f_0 is measured as described, first for the whole system, then with a short circuit across L_4, then across L_2, and finally for the whole system with L_2 removed. Since the capacity C is known, these measurements yield four equations which can be solved for the four inductances.

Available from

HER MAJESTY'S STATIONERY OFFICE

49 High Holborn, London, W.C.1
423 Oxford Street, London W.1
13a Castle Street, Edinburgh 2
109 St. Mary Street, Cardiff
Brazennose Street, Manchester 2
50 Fairfax Street, Bristol 1
35 Smallbrook, Ringway, Birmingham 5
80 Chichester Street, Belfast

or through any bookseller.

Printed in England

S. O. Code No. 91-3-19-85